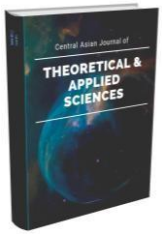

CENTRAL ASIAN JOURNAL OF THEORETICAL AND APPLIED SCIENCE

https://cajotas.centralasianstudies.org/index.php/CAJOTAS

Volume: 06 Issue: 03 | July 2025 ISSN: 2660-5317

Article

Comparative Analysis of Cu_2O:ZnO Nanocomposites Synthesized via Green and Sol-Gel Methods for Antibiofilm and Antibacterial Activities

Ali K. Hattab[1], Ali A. Fayyadh[2], Jawad N. K. Makassees[3]

1. Department of Physics, College of Science, University of Wasit, Wasit, Iraq.
2. Ministry of Education, General Directorate of Wasit Education, Wasit, Iraq.
3. Ministry of Education, General Directorate of Wasit Education, Wasit, Iraq.

* Correspondence: ahatab@uowasit.edu.iq , alia224@uowasit.edu.iq , jalmaksusse@uowasit.edu.iq

Abstract: The increasing prevalence of antibiotic-resistant bacteria, especially in biofilm-related infections, highlights the urgent need for innovative antimicrobial materials with effective mechanisms. This study presents a comparative analysis of Cu2O-ZnO nanocomposites synthesized via two distinct methods: a green synthesis approach employing extract of Curcuma longa (turmeric) rhizomes G-Cu_2O:ZnO and a sol-gel method SG-Cu_2O:ZnO. The nanocomposites were evaluated there antibiofilm and antibacterial properties. The relevance of the structural, optical, and morphological studies of the obtained nanocomposites was determined using XRD, FTIR, UV-Vis spectroscopy, and FESEM-EDX analysis. The nanocomposite sample synthesized using the green method exhibited better phase purity, uniform spherical morphology, and a smaller crystallite size range compared to those synthesized by the sol-gel method. The major distinctions are structural, where green synthesis gives a simpler binary phase structure and a better oxidation state control. The nanocomposites characterized efficient bacteria killing against both "Gram-positive and Gram- negative" bacteria as well as effective antibacterial activity against multi-drug-resistant bacterial species. The Uv-Vis optical properties, characterized by narrow bandgaps and localized surface plasmon resonance (SPR), enhance their antibacterial capabilities. Thus, functional groups identified by FTIR spectroscopy also support their antimicrobial property.

Keywords: Antibacterial, Antibiofilm, Green, Nanocomposite, Sol-gel

Citation: Hattab, A. K, Fayyadh, A. A & Makassees, J. N. K. Comparative Analysis of Cu2O:ZnO Nanocomposites Synthesized via Green and Sol-Gel Methods for Antibiofilm and Antibacterial Activities. Central Asian Journal of Theoretical and Applied Science 2025, 6(3), 315-328.

Received: 03th Mar 2025
Revised: 11th Apr 2025
Accepted: 24th May 2025
Published: 11th Jun 2025

1. Introduction

The emergence of diseases caused by antibiotic-resistant bacteria and the complications due to biofilm-associated infections are compelling people to look for new alternative means of combating bacterial infections[1]. In this regard, metal oxide nanoparticles especially Cu_2O and ZnO have received enormous attention because of their embedded physicochemical features and excellent antimicrobial properties[2]. Also, the nanocomposite shows better functionality than its individual counterparts; therefore, its potential use in biomedical applications[3], [4]. Nanocomposites and various products of biomedical fields using nanocomposites are considered to be one of the most rapidly growing and innovative areas in medicinal sciences. As can be seen, they are used in the making of drug/protein-releasing coatings on implants, tissue engineering scaffolds, and in a variety of diagnostic techniques[5]. The application of nanocomposites to biomaterials could make the diagnosis and treatment processes more effective and precise, and extend the service life of such biomaterials. It can be thus expected that inorganic/organic

biodegradable nanocomposite systems will be a key element of the present society[6]. Based on the available studies, scholars are expected to uncover a set of new products in the following years which would be designed with biodegradable nanocomposites. As a fast-growing field biomedical nanocomposites are successfully enhancing many works at present time. In this case, the drug is administered to the patients through tablets, capsules, and time-release formulations[7]. The reason why such synthesis methods have been selected is substantive. The green synthesis approach also incorporates the increasing focus on safer and greener ways of making nanomaterials that require fewer hazardous chemicals and potentially even better biocompatibility. In contrast, the sol-gel technique is a very precise technique of preparing the nanoparticles and tailoring the structure of nanoparticles can easily be varied to get the best physiochemical properties for a specific application[8]. Kandav et al. (2024) synthesized metallic nanoparticles employing the green synthesis method using plant extracts, microorganisms, and biopolymers. This method is green, economical, reproducible, and versatile enabling applications in catalysis, medicines, and energy-related technologies[9]. Oleiwi et al. (2022) conducted evaluation for sol-gel and green synthesis to prepare TiO_2 Nanoparticles. The TiO_2 nanoparticles were analyzed for crystallite size, functional groups, optical properties, and morphology [10]. Kohili et al. (2025) sustainable preparation of carbon quantum dots (CQDs) using green synthesis approach from natural raw materials offers a sustainable and biocompatible approach for diverse applications[11].The antimicrobial activity involves the bacterial strain isolation, identification, evaluation of minimum inhibitory concentration(MIC), sub-MIC, biofilm, antibiofilm, and antibacterial activities using the agar well diffusion method, providing a reliable method for analyzing the properties of the nanocomposite[12], [13], [14], [15], [16]. The present work aims to investigate the preparation of Cu_2O:ZnO nanocomposite through green synthesis and sol-gel approaches. In the green synthesis, the metal nanoparticles are reduced and stabilized by *Curcuma longa* (turmeric) rhizomes, an excellent environment-friendly molecule; while sol-gel derivatization provides better control over the nanoparticle size and composition. This study demonstrates how Cu_2O:ZnO nanocomposites can be used in biomedical applications to combat microbial resistance and biofilm formations further in the development of nanomaterial-based on metal oxides.

2. Materials and Methods

2.1. Materials

Copper nitrate trihydrate $Cu(NO_3)_2{\cdot}3H_2O$ functioned as the precursor material during the synthesis of Cu_2O:ZnO nanocomposite. Copper (Cu) of 99% with (Cl^-) ≤ 0.003%, (SO_4^{2-}) ≤ 0.01%, (Fe) ≤ 0.01%, (Pb) ≤ 0.05%, and (hydrogen sulfide) ≤ 0.1% impurities. Zinc nitrate hexahydrate $Zn(NO_3)_2{\cdot}6H_2O$ with (Zn) of 98 % with (HNO_3) ≤ 0.05%, (SO_4^{2-}) ≤ 0.005%, (Fe) ≤ 0.001%, (Cl^-) ≤ 0.005%, (Pb) ≤ 0.002% impurities. Both materials are from Thomas Baker, India. *Curcuma longa* extract was obtained from turmeric rhizomes.

2.2. Methods

2.2.1. Synthesize of Cu_2O: ZnO nanocomposite using green method

Preparation of Plant Extract: *Curcuma longa* extract was obtained from turmeric rhizomes and evaluated in the dried form and ground into fine powder. From the powder, 1 gram was weighed and in a clean beaker, 2 grams of the powder was dissolved in 100 mL DI water. The system was thermally stabilized at 50 °C for 1 hour with continuous stirring at 700 rpm to facilitate the extraction of *Curcuma longa*. A heating process was followed by cooling to room temperature naturally, then filtered using vacuum filtration method utilizing filter paper to separate residues. The filtrate, which contains *Curcuma longa* extract, was used in the synthesis as a natural stabilizing and reducing agent.

Green Synthesis: Under vigorous stirring of 700 rpm at 25 °C for one hour, one molar of copper nitrate trihydrate and zinc nitrate hexahydrate solutions were dissolved in separate beakers containing 50 ml of distilled water. Combining the two solutions to create a homogeneous mixture of copper and zinc nitrates. Slowly add the *Curcuma longa* extract to the combined solution while continuously stirring, allowing *Curcuma longa* extract to act as a stabilizing and reducing agent for both copper and zinc ions.

by dropping in NaOH, to increase the solution pH to an alkaline region of ~12 to encourage the precipitation of metal oxides. Hint: At this point, stirring the reaction mixture for one hour, at an average temperature of 70-80 °C, would be cleared. The formation of the G-Cu_2O: ZnO nanocomposite is a sign of a color change to the green solution. The precipitate was cleaned, dried in the oven at 100 °C during 4 hours and calcined in 500 °C during 2 hours.

2.2.2. Synthesize of Cu_2O:ZnO nanocomposite using sol-gel method

The copper nitrate and zinc nitrate were dissolved in deionized water, forming a clear solution with a light blue color. Then sodium hydroxide was added dropwise while stirring the solution continuously, and the pH was maintained at ~12 to facilitate the formation of metal hydroxides with a cloudy blue color. The mixture was heated to 80 °C and stirred continuously, allowing the metal ions to undergo hydrolysis and condensation reactions, which resulted in the formation of a gel. Stirring continued until the gel became stable, indicating the complete transition from solution to gel with pale blue to bluish-gray color. The formed gel was then dried at 100 °C for 4 hours to remove any excess water and volatiles, leading to the formation of a dry, solid precursor. The dried gel was subsequently calcined at 500°C for 2 hrs. in furnace. This thermal treatment enabled the decomposition of metal hydroxides into their respective oxides, Cu_2O and ZnO, while promoting the crystallization of the SG-Cu_2O: ZnO nanocomposite material.

2.2.3. Isolation and Identification of Bacterial Strains

Four types of bacteria strains were isolated and identified which are "*Staphylococcus aureus*, *Pseudomonas aeruginosa*, *Klebsiella pneumoniae*, and *Entercoccus faecalis"*, clinical specimens are collected from appropriate sources such as pus, wound swabs, sputum, urine, and blood. For *S. aureus*, samples are inoculated onto Mannitol Salt Agar (MSA), which selects for *Staphylococcis* and distinguishes *S. aureus* according to the fermentation of mannitol that produces yellow colony after 24 hours of incubation at 37 °C. Identification is confirmed using microscopy, catalase, coagulase tests, and further biochemical tests like DNase production and mannitol fermentation. For *P. aeruginosa*, samples are cultured on *Pseudomonas* Isolation agar and incubated at 37 °C for 24 hours. Identification involves microscopy, gram staining, catalase, oxidase, and fluorescence tests, with pyocyanin production (a blue-green pigment) as a key characteristic. *K. pneumoniae* is cultured on MacConkey Agar, incubated at 37 °C for 24 hours, and identified by Gram staining, lactose fermentation, and biochemical tests such as urease, indole, and hydrogen sulfide production. *E. faecalis* samples are inoculated onto *Enterococcal* Agar, sometimes supplemented with bile salts, and incubated at 37 °C for 24 hours. Identification is performed using gram staining, catalase, bile esculin tests, and growth in high salt concentrations.

2.2.4. Minimum Inhibitory Concentration (MIC) and sub-MIC

The determination of minimum inhibitory concentration(MIC) and sub-MIC for bacterial isolates is determined for "*S. aureus*, *P. aeruginosa*, *K. pneumoniae*, and *E. faecalis"*, perform double serial dilutions using the following procedure. Prepare two antibiotics in double serial dilutions, ranging from 1 to 1024 μg/mL, by diluting a stock solution (10 mg/mL) in Mueller-Hinton broth on a microtiter plate. Inoculate each well with 20 μL of bacterial suspension, ensuring the suspension matches McFarland turbidity standard (~ 1.5×10^8 CFU/mL) no. 0.5. For negative control wells, do not add any bacterial suspension. Incubate the microtiter plates at 37°C for 18-20 hours. After incubation, add 20 μL of resazurin dye to each well, which will indicate bacterial viability. Incubate the plates for an additional 2 hours at 37 °C. After this second incubation, observe the wells for color changes. A shift from blue to pink indicates bacterial growth, while wells that remain blue suggest inhibition, indicating the MIC.

2.2.5. Biofilm and Antibiofilm Activity

The biofilm and antibiofilm activities of both nanocomposites were evaluated against four bacterial strains: "*S.aureus*, *P.aeruginosa*, *K.pneumoniae*, and *E.faecalis"*. Bacterial cultures were prepared by inoculating each strain in LB broth, followed by incubation at for 16-18 hours at 37 °C. Both nanocomposites were dissolved in PBS or DMSO at concentrations varying between 10 and 100 μg/mL and sterilized by filtration. For the biofilm formation, 100 μL of each bacterial suspension (10^6 CFU/mL) was added to a 96-well microplate and incubated at 37 °C for 24 hours to allow biofilm formation.

Once the incubation had been completed, specific planktonic cells were carefully harvested, and the wells rinsed using PBS to clear any residual floating cells. In the antibiofilm assay, 100 μL of either G- Cu_2O:ZnO nanocomposite or SG-Cu_2O:ZnO nanocomposite solution was added to wells containing pre-formed biofilms, and the plate was incubated for an additional 24 hours at 37 °C. Control wells included untreated bacteria (positive control) and nanocomposite solutions without bacteria (negative control). Quantification of the biofilm after treatments was done using staining method with crystal violet. Wells were washed, stained with 0.1% violet crystal during 15 min, washed again and dissolved with ethanol or acetic acid. Absorbance was measured at 570 nm using a microplate reader to quantify biofilm formation. To identify the minimum biofilm inhibitory concentration($MBIC_{50}$), serial dilutions of the nanocomposites were tested to find the lowest concentration that inhibited at least 50% of biofilm formation. Finally, data were analyzed to compare the antibiofilm activity of G-Cu_2O:ZnO nanocomposite and SG-Cu_2O:ZnO nanocomposite for each bacterial strain, determining which nanocomposite and concentration exhibited the greatest biofilm inhibition.

2.2.6. Antibacterial Activity

The agar well diffusion method was utilized to assess the antibacterial activity of G-Cu_2O:ZnO nanocomposite and SG-Cu_2O:ZnO nanocomposite against the four bacterial at the MIC concentration. Each bacterial isolate was grown in nutrient broth for (18-24) hours at 37 °C. Following this, each bacterial suspension was spread on nutrient agar plates and 0.1 mL of each suspension was placed on a plate and the plates were incubated at 37 °C overnight (24 hours). A single colony was transferred to 5 mL of normal saline to achieve a turbidity of approximately 1.5×10^8 CFU/mL. Utilizing a sterile cotton swab, the bacterial suspension was evenly spread on Mueller-Hinton agar plates and left to dry for 10 minutes. Wells (5 mm in diameter) were created in the agar, and 50 μL of nanocomposites were added to each well, with distilled water as a control. They incubated the plates at 37 °C (18 hours). Following the incubation, the inhibition zone diameters were determined.

2.2.7. Characterization Techniques

Techniques including different analytical methods were used to analyze the Cu_2O-ZnO nanocomposites that were synthesized. A Bruker D8 Advance diffractometer with Cu Kalpha (λ = 1.54060 Å) radiation-X-ray Diffraction (XRD), worked under 45 kV and 35 mA voltage. The characterization of crystalline sample phases occurred by collecting data from 5° to 85° 2θ at a step size of 0.015° and a scan rate of 1.5°/min. The formation of metal–oxygen bonds together with functional group detection was investigated using an FT-IR spectroscopy system operated from the Thermo Scientific Nicolet iS5 spectrometer. The spectra measured from 4000–400 cm^{-1} using Attenuated Total Reflectance(ATR) enabled measurement through the solid sample without KBr pellets. The identification of the Cu-O and Zn-O stretching vibrations through spectrometry analysis were used to confirmed the successful synthesis of the nanocomposites. A PerkinElmer Lambda 1050 UV-Vis-NIR spectrophotometer produced the optical characteristics readings of the nanocomposites. The absorption spectra measurement took place from 250–850 nm. A quartz cuvette held the distilled water solution containing the nanocomposites which underwent sonication until they formed a uniform colloid before measurement. An optical band gap determination was made possible by drawing a Tauc plot with $(\alpha h\nu)^2$ against photon energy (hv) while utilizing the absorption coefficient value computed from the absorbance measurements. A JEOL JSM-7610F microscope under 15 kV conditions performed Field Emission Scanning Electron Microscopy (FESEM) tests to study the surface characteristics along with particle dimensions and structural elements at multiple magnification levels. The FESEM system incorporated EDX mode to analyze elemental composition and its 25 kV operation allowed detection of copper (Cu) zinc (Zn) and oxygen (O) signatures. The atomic analysis of Cu to Zn affirmed the proper nanocomposite formation and stoichiometric ratio of the Cu_2O-ZnO material.

3. Results and Discussion

X-ray diffraction (XRD) serves as the method to analyze the crystal structures in the synthesized products. The interplanar lattice spacing d can be determined through application of Bragg's law formula Equation 1 [17].

$$n\lambda = 2d \sin\theta \text{ ..... } 1$$

The X-ray diffraction process depends on four measurements including peak order n, incident wavelength λ, interplanar spacing d, and incidence angle θ. Knowing the interplanar spacing depends on the foundation between n and λ to determine d for various crystal structures. Equation 2 of Debye-Scherer provided the calculations for average crystallite size. The method allows scientists to determine the dimensions of crystal fragment specimens.

$$D = (k\lambda)/(\beta \cos\theta) \text{ ..... } 2$$

The X-ray crystallite size D expressed in nanometers can be calculated through the equation using the form factor K (0.94), wavelength λ (0.154060 nm), Bragg diffraction angle θ (Radian) and the Full Width at Half Maximum (FWHM) β (Radian) of the selected peak [18]. The X-ray diffraction (XRD) patterns of G-Cu_2O:ZnO nanocomposite and SG-Cu_2O:ZnO nanocomposite are shown in Fig. 1. The comparison of these nanocomposites provides insights into the structural characteristics, phase composition, and crystallite sizes of the resulting nanocomposites. The XRD patterns of G-Cu_2O:ZnO nanocomposite revealed Cu_2O cubic crystalline structure described in the entry crystallography open database (COD) [96-101-0942] along with hexagonal crystalline structure of ZnO based on entry cod [96-230-0116]. Three prominent peaks detected at 35.027°, 36.51° and 57.45° reveal crystallite dimensions of 24.32 nm from the (002) plane and 22.94 nm from (111) together with 23.13 nm from (110) [19].

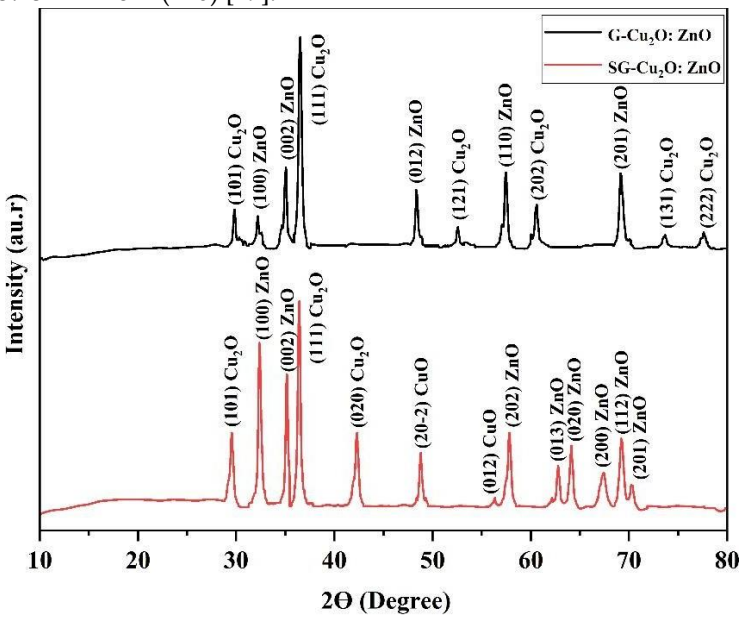

Figure 1. XRD pattern of G-Cu_2O:ZnO and SG-Cu_2O:ZnO nanocomposites.

The XRD patterns of SG-Cu_2O:ZnO nanocomposite identified a cubic and monoclinic crystal structure of Cu_2O and CuO according to the [96-900-5770] and [96-410- 5683] entry cod, respectively. Also, a hexagonal crystal structure of ZnO according to the [96-230-0117] entry cod. The three strongest peaks (2θ); 32.39°, 35.16°, and 36.41° correspond to planes and crystallite sizes of (100) plane: 25.55nm, (002) plane: 28.69 nm, and (111) plane: 25.95 nm, respectively[20]. Both methods produce nanocomposites containing Cu_2O and ZnO phases. The sol-gel method additionally shows monoclinic CuO, indicating partial oxidation of Cu_2O, while the green synthesis method favors Cu_2O formation without CuO. The sol-gel method yields slightly larger crystallites (26.73 nm) compared to green synthesis (23.46 nm), suggesting more extended crystal growth.

Differences in peak orientations indicate variations in crystal growth, with green synthesis showing the strongest peak at 36.51° (111) for Cu_2O, and sol-gel at 32.39° (100). Both methods yield hexagonal ZnO, with slight structural differences. The sol-gel method produces a more complex CuO/ Cu_2O system, while green synthesis favors a binary Cu_2O nanocomposite. The sol-gel method offers mixed copper oxide phases for tunable properties, while green synthesis provides better control over phase purity and oxidation state. The FESEM images in Fig. 2 (a-b) show the surface morphology of the synthesized samples G- Cu_2O:ZnO nanocomposite (SG-Cu_2O:ZnO nanocomposite, respectively. The G-Cu_2O:ZnO nanocomposite reveals several distinct morphological characteristics when compared to the SG-Cu_2O:ZnO nanocomposite. The particles in the SG-Cu_2O:ZnO sample have a larger size and more angular structure compared to that of G-Cu_2O:ZnO particles which are more uniform and nearly spherical. This irregularity causes a highly non-uniform particle morphology with clearly distinguishable changes in the particle shape and size. Additionally, the SG-Cu_2O:ZnO particles gave a higher average particle size of 63.23 nm and a broader size distribution that suggests a wider variation in the diameters of particles. In terms of surface texture, the SG-Cu_2O:ZnO particles appear to be somewhat more irregular, perhaps due to the sol-gel synthesis method, which can impose further surface imperfections and asymmetries. The packing density of the nanoparticles in this sample is also notably higher, with fewer void spaces between particles, suggesting a more compact arrangement that might lead to a reduced overall surface area compared to the SG-Cu_2O:ZnO nanocomposite. The green synthesis of G-Cu_2O:ZnO nanocomposite provides improved spherical morphology with a narrow particle size distribution of ZnO with an average particle size of 55.42 nm size. Its surface pH texture and more porous packing arrangement could be advantageous for applications that benefit from higher surface area and accessibility. Conversely, the sol-gel synthesized nanocomposite sample, displays a broader particle size distribution, rougher surface texture, and denser packing. These differences, likely due to the sol-gel process, may introduce structural variations and defects, impacting its catalytic activity, adsorption capacity, and overall functional properties. These morphological differences have demonstrated the dependency of the synthesis methods on the applicational performance of the nanocomposites.

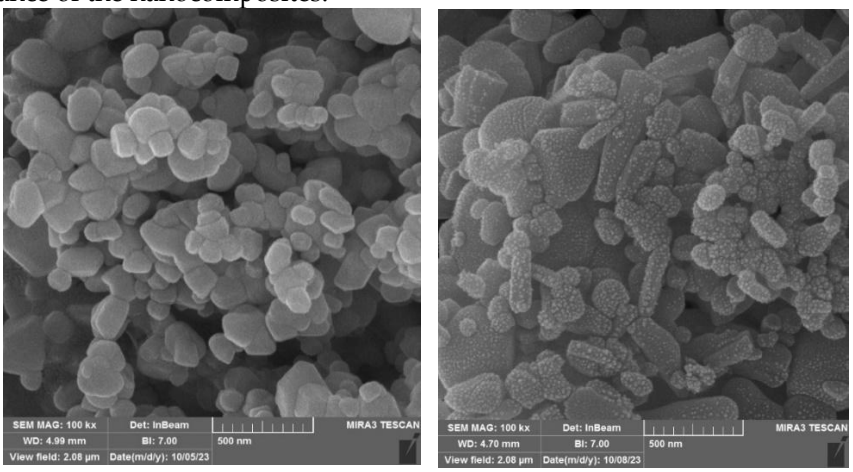

Figure 2. FESEM images of (a-left) G-Cu_2O:ZnO and (b-right) SG-Cu_2O:ZnO nanocomposites.

Fig. 3 a and b show the energy-dispersive X-Ray (EDX) spectrum of G-Cu_2O:ZnO nanocomposite and SG-Cu_2O:ZnO nanocomposite, respectively. Also give a quantitative result corresponding to copper, zinc, and oxygen elements in a weight percentage (W%) and an atomic weight percentage (A%) of the synthesized samples. The EDX spectrum of G-Cu_2O:ZnO nanocomposite sample confirms several elemental composition; Oxygen ($Ok_{\alpha 1}$) at 0.540 KeV with 31.17 W%; 59.86 A%, Copper (Cu $k_{\alpha 1}$): at 8.1 KeV with 40.20 W%; 19.44 A% and Zinc ($Znk_{\alpha 1}$) at 8.680 KeV with 25.17 W%; 11.83 A%, and Carbon (C): 3.47 W%; 8.87 A%.

The presence of Cu, Zn, and O confirms the formation of the Cu_2O: ZnO nanocomposite structure synthesis by the sol-gel approach. In the SG-Cu_2O:ZnO sample, EDX analysis shows Oxygen (O $k_{\alpha 1}$) with 25.98 W%, 40.91 A%; Copper (Cu $k_{\alpha 1}$)with 33.46 W%, 19.30 A%; Zinc (Zn $k_{\alpha 1}$) with 35.01 W%, 28.14 A% and Carbon (C $k_{\alpha 1}$) at with 5.55 W%, 11.64 A%[21,22]. In summary, both FESEM and EDX analyses validate the successful synthesis of G-Cu_2O:ZnO and SG-Cu_2O:ZnO nanocomposites. Overall, the EDX analysis confirms the successful formation of the Cu_2O:ZnO nanocomposite with some areas for potential optimization in terms of purity and particle dispersion.

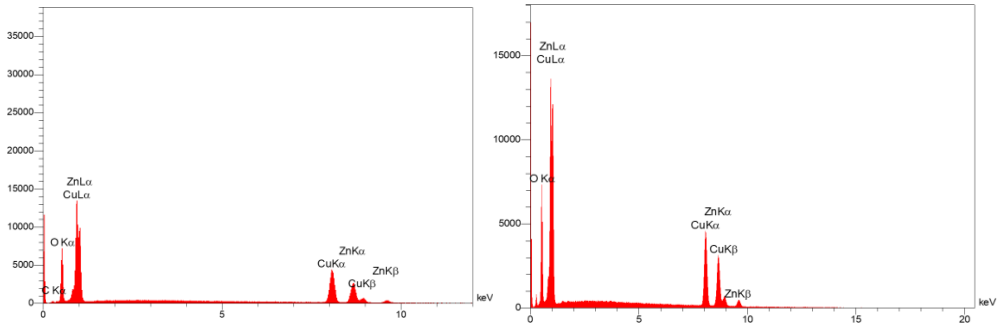

Figure 3. EDX spectrum of (a-left) G-Cu_2O:ZnO and (b-right) SG-Cu_2O:ZnO nanocomposites.

The optical properties of the nanocomposite samples were investigated using a UV-Vis spectrophotometer. The absorption spectrum with the wavelength range (190-1100 nm) of the electromagnetic spectrum and energy bandgap for the direct electronic transitions of the G-Cu_2O:ZnO and SG-Cu_2O:ZnO nanocomposites shown in Fig. 4 a and b, respectively. They are revealing similar optical and electronic properties with significant implications for biological applications. Both nanocomposites demonstrate nanocrystalline characteristics, with G-Cu_2O:ZnO displaying an absorption peak at 521 nm and SG-Cu_2O:ZnO at 522 nm, falling in the green region of the visible spectrum (495-570 nm). The direct allowed energy bandgap (E_g) is accessed using Tauc's equation 3 by plotting $(\alpha h\upsilon)^2$ vs $h\upsilon$ via extrapolating a straight line on the energy axis[23].

$$\alpha h\upsilon = B\,(h\upsilon - Eg)^r \quad \ldots\ldots\ldots 3$$

Here: Eg is the energy gap between direct transitions, B is a constant dependent on the material type, $h\upsilon$ is photon energy, equal to 1240 eV /λ, and the power coefficient is symbolized by r; The computation is based on potential electronic transitions, where a factor of (1/2) represents direct allowed transitions, while (3/2) represents a direct forbidden transition. The energy bandgap values of 2.12 eV for G-Cu_2O: ZnO and 2.10 eV for SG-Cu_2O:ZnO indicate strong visible light absorption, efficient electron-hole pair generation, and enhanced photocatalytic activity, all of which are advantageous for antibacterial and antibiofilm functions. In terms of antibacterial activity, the narrow bandgaps facilitate efficient visible light absorption, driving electron-hole pair generation and producing reactive oxygen species (ROS) crucial for bacterial inhibition. The localized surface plasmon resonance (SPR) at 521-522 nm contributes to enhanced interaction with bacterial membranes, localized heating, and improved cell penetration. For antibiofilm applications, the low bandgaps and strong visible light absorption allow continuous ROS generation under light exposure, disrupting biofilm formation, degrading existing biofilms, and preventing bacterial adhesion through surface modification. The optical properties also influence the minimum inhibitory concentration(MIC) values, as the narrow bandgaps reduce the concentrations needed for effective bacterial inhibition, support faster antimicrobial action, and maintain continuous ROS production. This continuous ROS generation ensures consistent antibacterial efficacy under visible light, effectively enhancing bacterial growth inhibition. Mechanistically, absorption at 521-522 nm activates photocatalytic processes, with bandgaps of 2.12/2.10 eV allowing efficient electron-hole separation and sustained ROS generation. SPR effects improve bacterial

membrane penetration, allowing photogenerated species to cause cellular damage, while photocatalytic activity further prevents bacterial adhesion and biofilm formation through surface interactions and ROS-based degradation. The practical advantages include visible light activation without UV requirements, making the materials safe for biological use, and comparable bandgaps and SPR peaks indicating similar performance across both nanocomposites. Their strong visible light absorption and antimicrobial capabilities render them versatile for medical applications, functioning effectively in varied lighting conditions and compatible with current treatment protocols. The slight differences in bandgap (2.12 vs. 2.10 eV) and absorption peak positions (521 vs. 522 nm) suggest that both synthesis methods produce materials of similar effectiveness, with the green synthesis (G-Cu_2O:ZnO) offering an environmentally friendly alternative to sol-gel synthesis (SG-Cu_2O:ZnO) while retaining comparable optical and antimicrobial properties. Together, these nanocomposites emerge as promising candidates for antibacterial, antibiofilm, and other photochemical applications in medical settings.

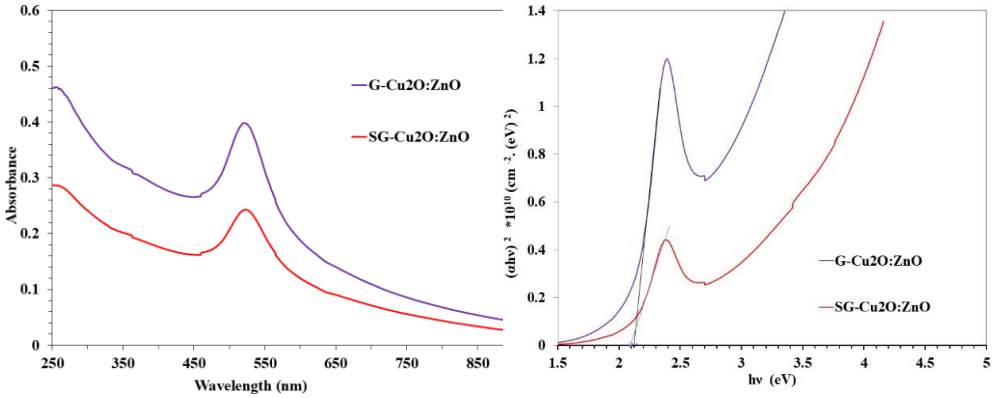

Figure 4. Optical properties (a-left) Uv-Vis absorption spectrum and (b-right) Energy bandgap (E_g) of G-Cu_2O:ZnO and SG-Cu_2O:ZnO nanocomposites.

Fourier Transform Infrared Spectroscopy(FTIR) was utilized to investigate the functional groups and chemical bonds of the nanocomposite samples. The FTIR spectra shown in Fig. 5 reveal significant functional groups that directly correlate with their biological activities of the G-Cu_2O:ZnO and SG-Cu_2O:ZnO nanocomposites. The characteristic of the absorption spectra bands in the range of 400-4000 cm^{-1}, with both samples exhibiting similar patterns but with slight shifts in peak positions, indicating successful synthesis through different methods. The prominent O-H stretching vibrations observed at 3443 cm^{-1} (G-Cu_2O:ZnO) and 3441 cm^{-1} (SG-Cu_2O:ZnO) are crucial for biological applications as these hydroxyl groups facilitate the generation of reactive oxygen species(ROS), which play a vital role in antimicrobial activity and biofilm disruption[24]. The presence of C-H stretching vibrations at 2934/2931 cm^{-1} and bending modes at 1388/1383 cm^{-1} suggests organic moieties that may contribute to the material's biocompatibility and interaction with bacterial cell membranes. Particularly significant for antimicrobial applications are the metal-oxygen vibrations observed at lower wavenumbers (532/488 cm^{-1}), which correspond to Cu-O and Zn-O bonds [25]. These metal-oxygen bonds are essential for the controlled release of Cu^{2+} and Zn^{2+} ions, which are fundamental to the materials' antibacterial mechanism through bacterial cell membrane disruption and metabolic interference. The bands at 1074/1068 cm^{-1}, attributed to C-O stretching, may enhance the materials' interaction with bacterial biofilms. These functional groups collectively contribute to the material's effectiveness in minimum inhibitory concentration(MIC) studies by facilitating multiple antibacterial mechanisms, including ROS generation, ion release, and membrane interaction. For biofilm and antibiofilm activities, the presence of surface hydroxyl groups and metal-oxygen bonds is particularly important as they enable penetration into biofilm matrices and prevent bacterial adhesion.

The slight variations in peak positions between the two samples suggest different coordination environments that might influence their biological efficacy, particularly in terms of ion release rates and ROS generation capacity. This comprehensive functional group analysis supports the materials' potential as effective antimicrobial agents through multiple simultaneous mechanisms of action, making them promising candidates for various biological applications requiring bacterial growth inhibition and biofilm control.

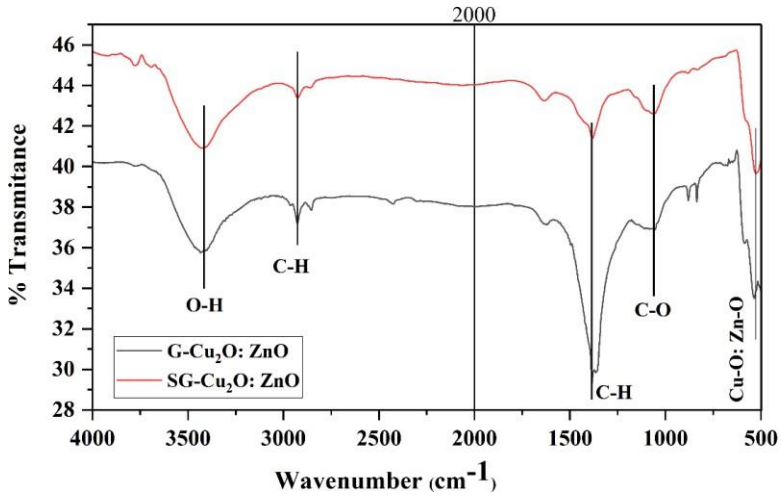

Figure 5. FTIR spectra of G-Cu2O:ZnO and SG-Cu2O:ZnO nanocomposites.

Isolation Efficiency and Bacterial Identification Outcomes: Isolation and identification of bacterial strains are conducted as follows: *S. aureus* is typically isolated from wound infections, skin abscesses, or nasal swabs. It is seen as Gram positive cocci (clusters) on Gram staining and forms yellow, beta-hemolytic colonies on blood agar. Confirmation involves positive catalase, coagulase, DNase tests, and mannitol fermentation on MSA. *P. aeruginosa* is isolated from respiratory, burn, or urinary tract infections. It shows Gram-negative rods on staining, produces a greenish- blue pigment (pyocyanin) on nutrient agar, and has a grape-like odor. It is oxidase- positive, motile, and grows on *Pseudomonas* Isolation Agar. *K. pneumoniae* is obtained from sputum, urine, or wound samples. It shows Gram-negative rods and forms large, mucoid, lactose-fermenting (pink) colonies on MacConkey agar. It is non-motile, urease-positive, and produces hydrogen sulfide. *E. faecalis*, often isolated from UTIs, blood, or wound infections, appears as Gram-positive cocci in pairs or chains. It grows in 6.5% NaCl, turns bile-esculin agar black, and is frequently resistant to multiple antibiotics.

Evaluation and Antibacterial Activity of MIC and sub-MIC: Table 1 presents the MIC and sub-MIC evaluations of G-Cu2O:ZnO and SG-Cu2O:ZnO nanocomposites. For *S. aureus*, the MIC for SG-Cu2O:ZnO nanocomposite was 32 μg/mL, with a sub-MIC of 16 μg/mL, while G-Cu2O:ZNO nanocomposite demonstrated lower values of 8 μg/mL (MIC) and 4 μg/mL (sub-MIC). This indicates that G-Cu2O:ZnO nanocomposite is more effective at inhibiting growth. Similarly, *P. aeruginosa* showed MIC values of (32 and 16) μg/mL for SG-Cu2O:ZnO nanocomposite, whereas G- Cu2O:ZnO nanocomposite had values of MIC equal 16 μg/mL and sub-MIC equal 8 μg/mL, indicating higher antibacterial activity of G-Cu2O:ZNO nanocomposite. In the case of *K. pneumoniae*, SG-Cu2O:ZnO nanocomposite had MIC and sub-MIC values of (32 and 16) μg/mL respectively; nevertheless, G-Cu2O: ZNO exhibited much better efficacy, with MIC and sub-MIC values of 16 μg/mL and 8 μg/mL respectively. For *E. faecalis*, both nanocomposite samples exhibited equal MIC and sub-MIC of (8 and 4) μg/mL against this bacterium so there is no significant difference in the efficacy of both the nanocomposites. Overall, G-Cu2O:ZnO nanocomposite is more effective than SG-Cu2O:ZnO nanocomposite against Gram positive *S.aureus*, Gram negative *P.aeruginosa*, and *K.pneumoniae* bacterium as suggested by the lower MIC.

However, for *E. faecalis*, both materials exhibit similar antibacterial effects. The enhanced efficacy of G-Cu_2O:ZnO nanocomposite may be attributed to its composition and structural properties, leading to more efficient bacterial inhibition.

Table 1. MIC and sub-MIC of G-Cu_2O:ZnO and SG-Cu_2O:ZnO nanocomposites.

The bacterial isolates	G-Cu_2O:ZnO nanocomposite (μg⁄ml)		SG-Cu_2O:ZnO nanocomposite (μg⁄ml)	
	MIC	Sub-MIC	MIC	Sub-MIC
S. aureus	8	32	16	4
P. aeruginosa	16	32	16	8
K. pneumoniae	16	32	16	8
E. faeclis	8	8	4	4

Evaluation of Biofilm and Antibiofilm Activity: The analysis of biofilm and antibiofilm activity of the G-Cu_2O:ZnO and SG-Cu_2O:ZnO nanocomposites present in Table 2 showed that the ability of bacterial strains to form biofilm, and react to the inhibition processes has different levels among all the tested strains. The initial OD values (before treatment) were obtained to be ranging between 0.444 ± 0.040 to 0.792 ± 0.081 which shows the variation of capability of bacterial species to form biofilms. After treatment, both nanocomposites demonstrated a remarkable reduction in biofilm formation, with G-Cu_2O:ZnO nanocomposite demonstrating higher efficiency in combating all the bacterial strains with no exception when compared to SG- Cu_2O:ZnO nanocomposite. The G-Cu_2O:ZnO nanocomposite exhibited the highest efficiency in biofilm inhibition, achieving reduction rates of 77.98% for S. aureus (OD reduction from 0.595 to 0.131 ± 0.044), 75.13% for *P. aeruginosa* (from 0.792 to 0.197 ± 0.004), 73.77% for *K. pneumoniae* (from 0.694 to 0.182 ± 0.003), and 78.15% for *E. faecalis* (from 0.444 to 0.097 ± 0.004). In comparison, SG-Cu_2O:ZnO nanocomposite showed moderate but significant reduction rates of 51.60%, 45.58%, 36.89%, and 26.80% for the respective bacterial strains, with final OD values of 0.288 ± 0.137, 0.431 ± 0.100, 0.438 ± 0.067, and 0.325 ± 0.108.

Table 2. Biofilm and Antibiofilm Activity of G-Cu_2O:ZnO and SG-Cu_2O:ZnO nanocomposites.

The bacterial isolates	Before treatment OD Mean ∓ SD	After treatment OD Mean ∓ SD	
		G-Cu_2O:ZnO nanocomposite	SG-Cu_2O:ZnO nanocomposite
S. aureus	0.595 ± 0.048	0.131 ± 0.044	0.288 ± 0.137
P. aeruginosa	0.792 ± 0.081	0.197 ± 0.004	0.431 ± 0.100
K. pneumoniae	0.694 ± 0.146	0.182 ± 0.003	0.438 ± 0.067
E. faeclis	0.444 ± 0.040	0.097 ± 0.004	0.325 ± 0.108

The enhanced performance of G-Cu_2O:ZnO nanocomposite can be attributed to several factors, including better dispersion, smaller particle size, and increased surface area for bacterial interaction, leading to more efficient release of active ions. All treated samples were classified as non-adherent based on the ODc calculations, indicating that both treatments effectively prevent biofilm formation. This suggests that the nanocomposites successfully interfere with bacterial adhesion mechanisms and may disrupt the initial attachment phase of biofilm formation. The variation in effectiveness among bacterial strains might be due to differences in bacterial cell wall structure and biofilm composition, with *E.faecalis* and *S.aureus* showing higher sensitivity to treatment compared to *P.aeruginosa* and *K.pneumoniae*. The mechanism of action likely involves multiple pathways, including the release of Cu^{2+} and Zn^{2+} ions, generation of reactive oxygen species(ROS), disruption of bacterial cell membranes, and interference with the

non-adherent classification across all bacterial strains emphasizes the potential of these nanocomposites in preventing biofilm-associated infections. Nonetheless, more investigations are needed to target long-term stability, in vivo efficacy, and potential cytotoxicity would be valuable for developing practical applications. The consistent performance of both nanocomposites, particularly G-Cu_2O:ZnO nanocomposite, in preventing bacterial adhesion suggests promising applications in medical devices, implants, and other surfaces where biofilm prevention is crucial. This study provides strong evidence for the potential use of these nanocomposites as effective antibiofilm agents in various biomedical applications, with G-Cu_2O:ZnO nanocomposite showing particularly promising results for future development and implementation.

Evaluation of Antibacterial Activity: The antibacterial activity of Cu_2O:ZnO nanocomposites reveals several significant findings. According to the data presented in Table 3 outlines the diameter of inhibition zones (in millimeters) for various bacterial isolates when exposed to nanoparticles synthesized through two alternative ways: Sol-gel and green synthesis. Additionally, the antibacterial performance of these nanoparticles is compared to azithromycin (Azm) at a concentration of 15 mg/ml. Notably, the G-Cu_2O:ZnO nanocomposite produced through the green synthesis method consistently resulted in larger inhibition zones across all bacterial isolates compared to those synthesized via the sol-gel method. *E. faecalis* exhibited the largest inhibition zones for both preparations, measuring 30 mm for the SG-Cu_2O:ZnO nanocomposite and 33 mm for the G-Cu_2O:ZnO nanocomposite. In contrast, *P. aeruginosa* showed complete resistance to *azithromycin* (with no inhibition zone, marked as 0 R), yet was significantly inhibited by both nanocomposites. *K. pneumoniae* demonstrated the smallest inhibition zones when exposed to both nanocomposites among all tested bacterial isolates.

Table 3. Antibacterial activity of G-Cu_2O:ZnO and SG-Cu_2O:ZnO nanocomposites.

The bacterial isolates	**The diameter of the inhibition zone (mm)**		
	G-Cu_2O:ZnO nanocomposite (15 mg/ml)	SG-Cu_2O:ZnO nanocomposite (15 mg/ml)	*Azithromycin* (15 mg/ml)
S. aureus	20	25	18
P. aeruginosa	25	28	0 R
K. pneumoniae	15	20	10
E. faeclis	30	33	20

The G-Cu_2O:ZnO nanocomposite appears more effective in generating antibacterial activity compared to the SG-Cu_2O:ZnO nanocomposite as shown in Fig. 6, likely due to variations in particle size, shape, or surface properties. Furthermore, both nanocomposites exhibited broad-spectrum antibacterial activity against *S.aureus*, *E.faecalis* (Gram-positive) bacteria and *P.aeruginosa*, *K.pneumoniae* (Gram-negative) bacteria, suggesting their potential utility in combating antibiotic-resistant strains. The varying susceptibility of different bacterial species to the nanoparticles was also noted, with *E. faecalis* being the most susceptible and *K. pneumoniae* the least affected. The potential mechanisms underlying the antibacterial activity of both nanocomposites may include the generation of reactive oxygen species(ROS), disruption of bacterial cell membranes, and interference with bacterial metabolism. It is important to recognize that all tests were conducted at a single concentration (15 mg/ml), and further studies with varying concentrations would be valuable to determine minimum inhibitory concentrations and elucidate dose-dependent effects. Future research should explore the exact mechanisms of action, investigate potential synergistic effects with conventional antibiotics, and conduct in vivo studies to further assess the effectiveness and safety of these nanoparticles as antimicrobial agents, particularly those synthesized using the green method, showing promising broad - spectrum antibacterial activity.

These findings suggest potential applications in the development of new antimicrobial treatments, especially against antibiotic-resistant strains.

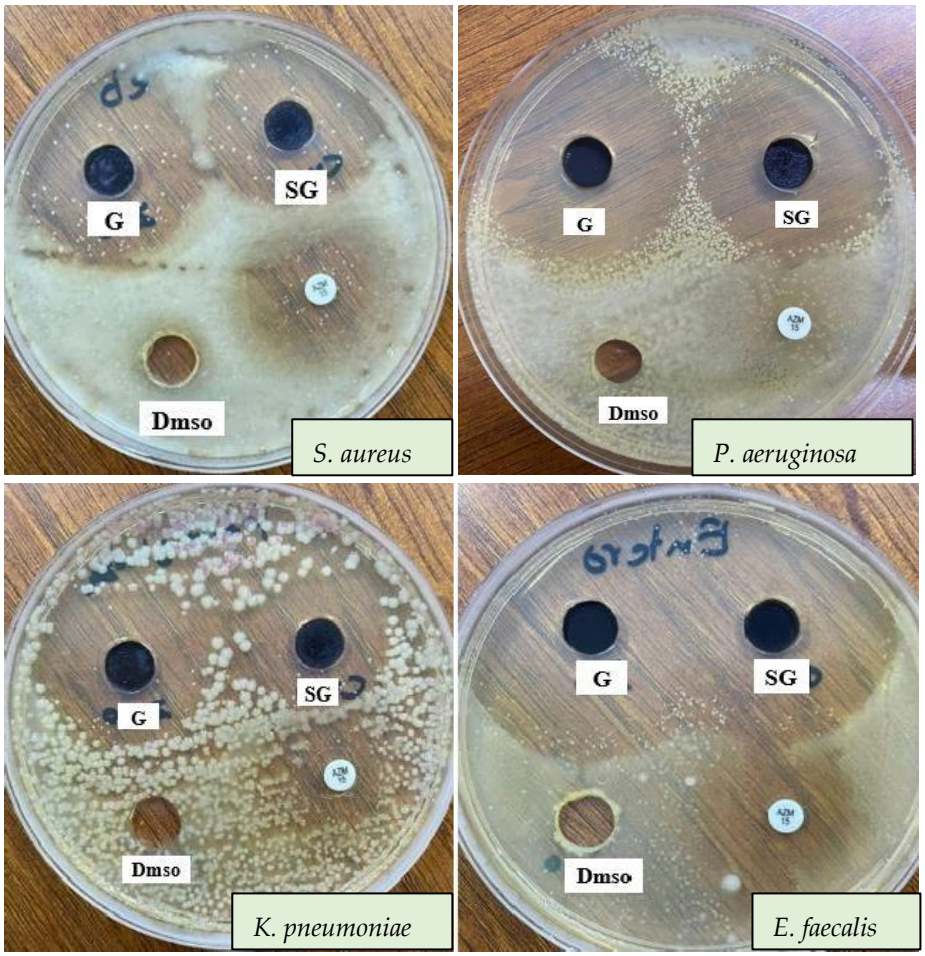

Figure 6. Antibacterial activity of G-Cu_2O:ZnO and SG-Cu_2O:ZnO nanocomposites.

4. Conclusion

The Cu_2O:ZnO nanocomposites were successfully synthesized using green and sol-gel methods with remarkable potential as innovative antibacterial and antibiofilm agents. The XRD analysis revealed that G-Cu_2O:ZnO exhibited a binary phase system with cubic Cu_2O and hexagonal ZnO structures, while SG-Cu_2O:ZnO showed an additional monoclinic CuO phase. FESEM images demonstrated that G-Cu_2O:ZnO possessed a more uniform, spherical morphology in the nanoparticle size range, compared to SG-Cu_2O:ZnO which shows a larger nanoparticle size range with more irregular particles. UV-Vis spectroscopy revealed comparable optical properties for G-Cu_2O:ZnO and SG-Cu_2O:ZnO nanocomposites, characterized by narrow absorption bands and localized surface plasmon resonance (SPR) within the visible region. The presence of nanocrystalline structure resulted in a red shift in the SPR peaks of both samples. Moreover, results revealed that the Eg reduced as a result of the excitonic effect and narrowing of the energy bandgap. The FTIR spectrum revealed functional groups: O-H stretching (3443/3441 cm-1) indicates ROS generation, while C-H vibrations (2934/2931 cm-1, 1388/1383 cm-1) support biocompatibility. Metal-oxygen vibration (532/488 cm-1) indicates Cu-O and Zn-O bonds vital for ion release. C-O stretching. The antibacterial activity of G-Cu_2O:ZnO nanocomposite against four human pathogenic bacterial strains. Demonstrated superior antibacterial activity with lower minimum inhibitory concentrations(MICs) ranging from(8-16) μg/mL, compared to (8-32) μg/mL for SG-Cu_2O:ZnO. Notably, G-Cu_2O:ZnO nanocomposite exhibited enhanced antibiofilm activity with reduction rates of 73.77-78.15% across all tested strains, significantly higher than the 26.80-51.60% reduction achieved by SG-Cu_2O:ZnO nanocomposite.

The results indicate that the green synthesis approach not only offers an environmentally friendly alternative but also produces nanocomposites with superior antimicrobial properties. These findings suggest potential applications in developing sustainable, efficient antimicrobial materials for medical applications, particularly in combating antibiotic-resistant bacterial infections and biofilm formation.

REFERENCES

[1] D. MubarakAli *et al*., "Recent Progress in Multifunctional Stimuli-Responsive Combinational Drug Delivery Systems for the Treatment of Biofilm-Forming Bacterial Infections," *Pharmaceutics*, vol. 16, no. 8, p. 976, 2024. doi: 10.3390/pharmaceutics16080976.

[2] C. Uthra *et al*., "Zinc and copper oxide nanoparticles: pioneering antibacterial and antibiofilm strategies for environmental restoration against antibiotic-resistant bacteria," *Materials*, vol. 17, no. 14, p. 3444, 2024. doi: 10.3390/ma17143444.

[3] P. H. Fathima Fasna *et al*., "Green Synthesis of CuO/ZnO Nanocomposites using Ficus Drupacea: In-Vitro Antibacterial and Cytotoxicity Analysis," *ChemistrySelect*, vol. 9, no. 22, p. e202401235, 2024. doi: 10.1002/slct.202401235.

[4] N. M. Khatir and A. K. Zak, "Antibacterial activity and structural properties of gelatin-based sol-gel synthesized Cu-doped ZnO nanoparticles; promising material for biomedical applications," *Heliyon*, vol. 10, no. 17, p. e37022, 2024. doi: 10.1016/j.heliyon.2024.e37022.

[5] M. El-Nablaway *et al*., "Prospectives and challenges of nano-tailored biomaterials-assisted biological molecules delivery for tissue engineering purposes," *Life Sci.*, p. 122671, 2024. doi: 10.1016/j.lfs.2024.122671.

[6] A. Prusty and S. Padhi, "Nanomaterials Marvels: Transformative Advancements in Biomedicine, Drug Delivery, and Pharmaceutical Analysis," *FABAD J. Pharm. Sci.*, vol. 49, no. 3, pp. 647–658, 2024. doi: 10.55262/fabadeczacilik.1520564.

[7] M. Geszke-Moritz and M. Moritz, "Biodegradable polymeric nanoparticle-based drug delivery systems: comprehensive overview, perspectives and challenges," *Polymers (Basel)*, vol. 16, no. 17, p. 2536, 2024. doi: 10.3390/polym16172536.

[8] F. Ahmed *et al*., "Green approaches in synthesising nanomaterials for environmental nanobioremediation: Technological advancements, applications, benefits and challenges," *Environ Res.*, vol. 204, p. 111967, 2022. doi: 10.1016/j.envres.2021.111967.

[9] G. Kandav and T. Sharma, "Green synthesis: an eco friendly approach for metallic nanoparticles synthesis," *Part. Sci. Technol.*, vol. 42, no. 5, pp. 874–894, 2024. doi: 10.1080/02726351.2023.2281452.

[10] H. F. Oleiwi *et al*., "Comparative Study of Sol-Gel and Green Synthesis Technique Using Orange Peel Extract to Prepare TiO_2 Nanoparticles," *Baghdad Sci. J.*, vol. 21, no. 5, pp. 1702–1711, 2022. doi: 10.21123/bsj.2023.8089.

[11] H. K. Kohli and D. Parab, "Green synthesis of carbon quantum dots and applications: An insight," *Next Materials*, vol. 8, p. 100527, 2025. doi: 10.1016/j.nxmate.2025.100527.

[12] A. S. G. Borges *et al*., "Fast identification method for screening bacteria from faecal samples using oxford nanopore technologies MinION sequencing," *Curr Microbiol*, vol. 80, no. 3, p. 101, 2023. doi: 10.1007/s00284-023-03201-7.

[13] L. Barnes *et al*., "Antimicrobial susceptibility testing to evaluate minimum inhibitory concentration values of clinically relevant antibiotics," *STAR Protoc.*, vol. 4, no. 3, p. 102512, 2023. doi: 10.1016/j.xpro.2023.102512.

[14] F. Sun *et al*., "Sub-minimum inhibitory concentration ceftazidime inhibits *Escherichia coli* biofilm formation by influencing the levels of the ibpA gene and extracellular indole," *J. Chemother.*, vol. 32, no. 1, pp. 7–14, 2020. doi: 10.1080/1120009X.2019.1678913.

[15] R. Chen *et al*., "An In Vitro Artificial Wound Slough–Biofilm Model Developed for Evaluating a Novel Antibiofilm Technology," *Microorganisms*, vol. 12, no. 11, p. 2223, 2024. doi: 10.3390/microorganisms12112223.

[16] G. Chavez-Esquivel *et al*., "Antimicrobial activity of graphite oxide doped with silver...," *Mater. Sci. Eng. C.*, vol. 123, p. 111934, 2021. doi: 10.1016/j.msec.2021.111934.

[17] F. Peng *et al*., "A new method for calculating interplanar spacing to distinguish between similar phases in EBSD," *J Microsc.*, vol. 291, no. 2, pp. 186–196, 2023. doi: 10.1111/jmi.13209.

[18] K. Mongkolsuttirat and J. Buajarern, "Uncertainty evaluation of crystallite size measurements of nanoparticle using X-Ray Diffraction analysis (XRD)," *J. Phys.: Conf. Ser.*, p. 012054, 2021. doi: 10.1088/1742-6596/1719/1/012054.

[19] X. Wang *et al*., "Photocatalytic activity of Cu_2O/ZnO nanocomposite for the decomposition of methyl orange under visible light irradiation," *Sci. Eng. Compos. Mater.*, vol. 26, no. 1, pp. 104–113, 2019. doi: 10.1515/secm-2018-0170.

[20] N. Widiarti, J. K. Sae, and S. Wahyuni, "Synthesis CuO-ZnO nanocomposite and its application as an antibacterial agent," *IOP Conf. Ser.: Mater. Sci. Eng.*, p. 012036, 2017. doi: 10.1088/1757-899X/172/1/012036.

[21] N. K. Pandey *et al*., "Relative Humidity Sensing Properties Of Cu_2O Doped ZnO Nanocomposite," *AIP Conf. Proc.*, pp. 463–466, 2009. doi: 10.1063/1.3183474.

[22] J. Zhang *et al*., "Copper doping and oxygen vacancy synergistic modification of zinc oxide nanosheets: Significantly improved antibacterial properties," *Mater Lett.*, p. 136777, 2024. doi: 10.1016/j.matlet.2024.136777.

[23] H. Zhong *et al*., "Idealizing Tauc plot for accurate bandgap determination of semiconductor with ultraviolet–visible spectroscopy: a case study for cubic boron arsenide," *J Phys Chem Lett.*, vol. 14, no. 29, pp. 6702–6708, 2023. doi: 10.1021/acs.jpclett.3c01416.

[24] R. Canaparo *et al*., "Biomedical applications of reactive oxygen species generation by metal nanoparticles," *Materials*, vol. 14, no. 1, p. 53, 2020. doi: 10.3390/ma14010053.

[25] D. V. Francis *et al*., "Antimicrobial activity of biogenic metal oxide nanoparticles and their synergistic effect on clinical pathogens," *Int J Mol Sci.*, vol. 24, no. 12, p. 9998, 2023. doi: 10.3390/ijms24129998